

Soft X-Ray EPMA analyses of nanophase lunar Fe-Si compounds

P. Gopon¹, J. Fournelle¹, J. Valley¹, W. Horn², P. Pinard³, P. Sobol¹, M. Spicuzza¹, X. Llovet⁴

¹Dept. of Geoscience, University of Wisconsin, Madison, Wisconsin USA

²ExxonMobil Research and Engineering Company, Annandale, New Jersey 08801 USA

³RWTH University, Aachen, Germany

⁴CCiTUB, University of Barcelona, Barcelona, Spain

Abstract

Conventional electron-probe microanalysis (EPMA) has an X-ray analytical spatial resolution on the order of 1-4 μm width/depth. Many of the naturally occurring Fe-Si compounds analyzed in this study are smaller than 1 μm in size, requiring the use of lower accelerating potentials and non-standard X-ray lines for analysis. The problems with the use of low energy X-ray lines (soft X-rays) of iron for quantitative analyses are discussed and a review is given of the alternative X-ray lines that may be used for iron at or below 5 keV (i.e., accelerating voltage that allows analysis of areas of interest smaller than 1 μm). Problems include the increased sensitivity to surface effects for soft X-rays, peak shifts (induced by chemical bonding, differential self-absorption, and/or buildup of carbon contamination), uncertainties in the mass attenuation coefficient (MAC) for X-ray lines near absorption edges, and issues with spectral resolution and count rates from the available Bragg diffractors. In addition to the results from the traditionally used Fe L α line, alternative approaches, utilizing Fe L β , and Fe L γ - η lines, are discussed.

Introduction

Conventional electron probe microanalysis (EPMA) uses high electron beam energies (15-20 keV) to eject inner shell electrons, and measures the characteristic photon energy emitted when an outer shell electron transitions into a vacant inner shell electron state. This technique is able to nondestructively and accurately determine the chemical composition of materials to within ~1% accuracy. The volume that the incident electron beam excites is directly proportional to the voltage of the incident beam and the material composition. At 20 keV a general depth/width of the incident electron scatter (in common geologic materials) is on the order of 1-4 μm (figure 1). Conventional EPMA is therefore not suited for analyses of features under 2 μm width, because the electron beam would cause excitation of electrons in atoms that are outside of the feature of interest. It has long been recognized that to properly analyze samples under 5 μm , it becomes necessary to use low voltage electron beams. However, this has been difficult with traditional tungsten source electron probes. With the development of field emission source electron probes, it is now possible to focus low voltage beams to sizes required for nanoscale features. Doing so introduces many complications such as changes in X-ray peak position/shape, surface contamination, and limited understanding of the mass absorption coefficients for low energy (soft) X-rays (Pouchou, 1996).

A recent study (Llovet et al., 2012) showed the difficulties of using L lines for quantitative EPMA. Some of the causes of these problems include changes in peak position/shape of the X-ray lines, increased sensitivity to surface contamination, and errors in accuracy of the tabulated

This research project was funded by the Wisconsin Space Grant Consortium. Additional support was provided by an ExxonMobil research grant. I would like to acknowledge Silvia Richter at RWTH Aachen, Michel Outrequin of CAMECA France, and Bill Horn of ExxonMobil Research and Engineering Corporation for the generous use of their electron microprobe facilities, without them this work would not have been possible.

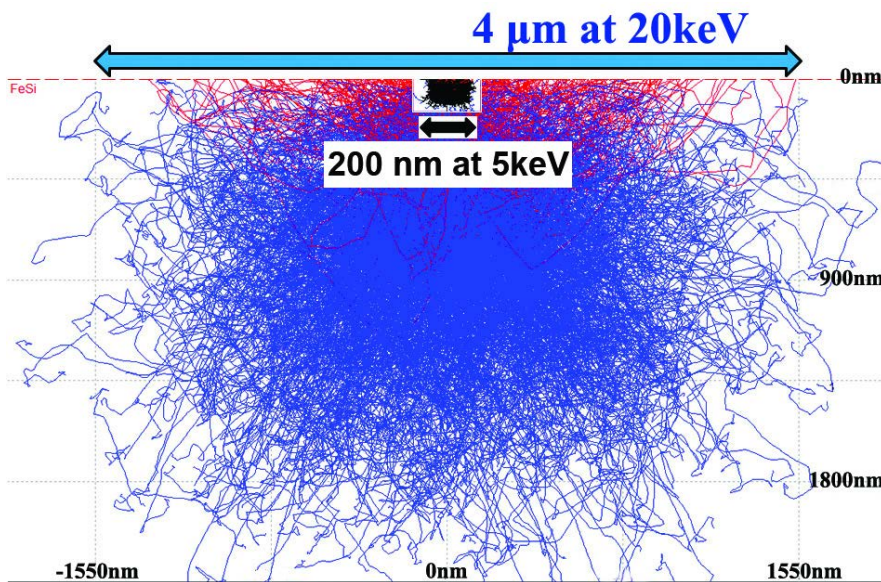


Figure 1: Monte Carlo simulation of the interaction volumes of a 5 keV (black) and 20 keV (blue) incident electron beam in FeSi. (using the CASINO software; Drouin et al, 2007)

mass attenuation coefficients (MACs) for low energy X-rays. The $L\alpha_{1,2}$ lines of the first-row transition metals are particularly problematic for quantitative analysis due to their proximity to their respective L_3 absorption edges. The $L\alpha$ transitions is between the M_5 and L_3 orbital (figure 2). The M_5 orbital is unfilled in the transition metals and is involved in bonding. This causes the $L\alpha$ transition to change energy depending on the bonding environment. Since even a small change of the X-ray line energy near absorption edges, changes the MAC by a large amount, this leads to large problems for quantitative analysis (figure 3).

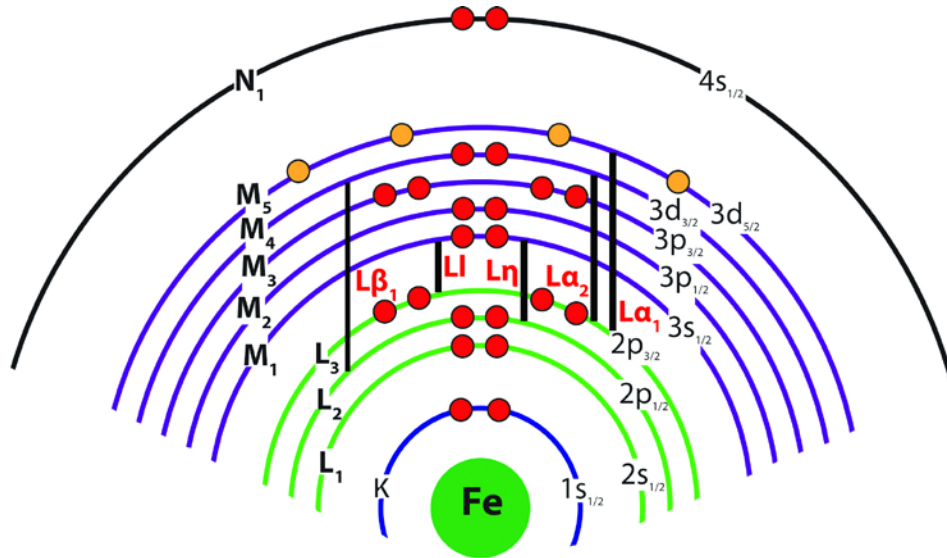


Figure 2: Schematic diagram of Fe electron cloud showing the major X-ray lines in Siegbahn and IUPAC notation, as well as the five transitions Fe $L\alpha_1$ $L\alpha_2$, $L\beta$, $L\gamma$, $L\eta$.

Objectives

This study's goal is to measure the chemistry of sub-micron iron-silicides found in lunar regolith believed to be associated with impact structures. These iron-silicides are of particular importance because of the extreme reducing conditions required for their formation. Analyses of lunar iron silicides has been attempted in the past by Anand, et al, 2004. However, analyses

were only done on the a small number of Fe-Si grains that were large enough for conventional analysis, due to the difficulty of analyses of sub-micron grains.

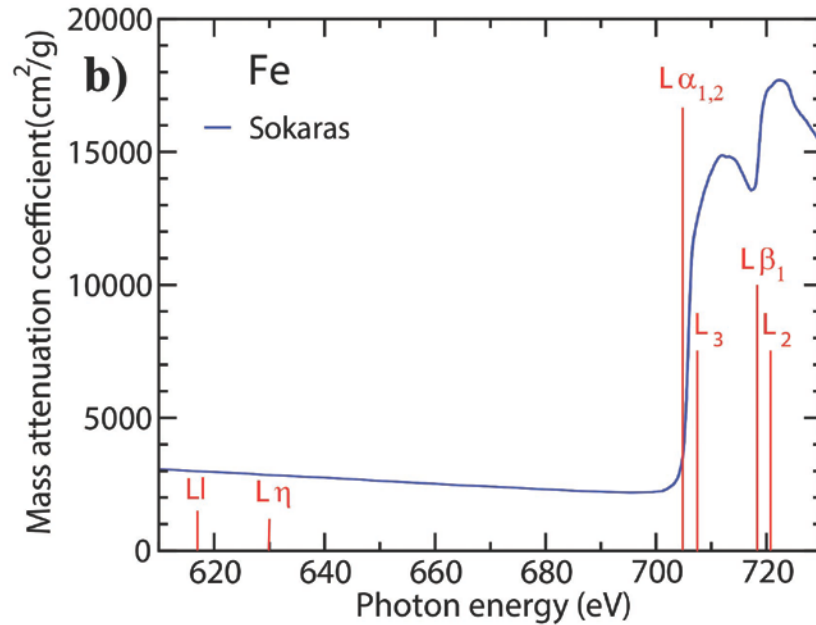


Figure 3: Experimental MAC's (taken from Sokaras et al., 2010) at the energies around the Fe $L\alpha$, $L\beta$, $L\eta$ and $L\eta$ lines, overlain with the corresponding tabulated line energies, and L_3 and L_2 absorption edges (values taken from Deslattes et al., 2003)

The motivation for the current study was an attempt at a proper EPMA analysis on sub-micron lunar Fe-Si compounds reported by Spicuzza et al. (2011) in Apollo 16 lunar regolith grains A6-8 (figure 4) and A6-7. These are hypothesized to have formed in the reducing environment of the moon after micro-meteorite impacts (Annad et al., 2004). They are significant because of the extreme reducing conditions required for formation. While native iron is fairly common in lunar dust, native silicon and iron-silicides have been rarely found. This is due to the order of magnitude lower reducing conditions needed to reduce to native silicon, as compared to native iron. However, their small size ($< 1 \mu\text{m}$) precludes quantitative measurements using conventional EPMA.

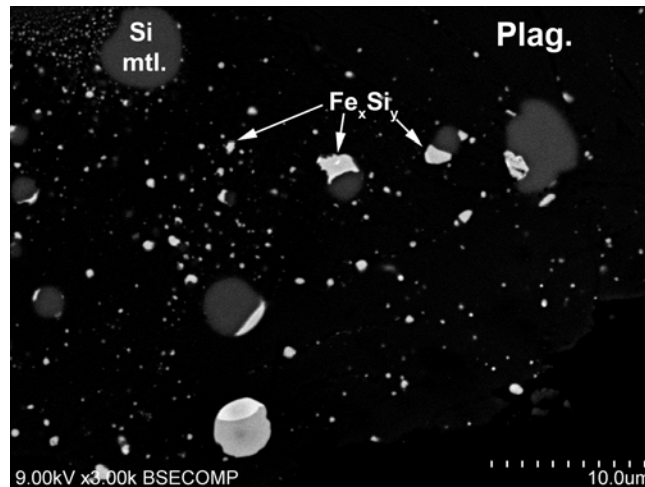


Figure 4: BSE image of plagioclase grain A6-8 from Apollo 16 regolith showing nano-phase Fe-Si compounds (bright phases), in a plagioclase matrix, the medium bright phases are silicon metal.

Background

These Fe-Si compounds are rarely found on Earth, the most notable example is in fulgarite deposit studied by Essene and Fisher (1986), but they do appear to be important in extraterrestrial bodies where highly reduced environments need for their formation are more common. Extra-terrestrial iron silicides have been described in samples collected from the comet Wild-2 (Rietmeijer, et al 2008), in iron-rich meteorites, and lunar impact environments. Such lunar impact iron-silicides were identified by Spicuzza et al. (2011) in a shocked plagioclase grain (grain A 6-8) from Apollo 16 lunar regolith sample 61501,22. However, due to the small size of the iron silicides (0.1-2 μm) chemical analyses of the Fe-Si compounds was not possible with conventional EPMA (15 keV). When soft X-ray EPMA (5 keV) was attempted on these lunar Fe-Si compounds, highly erroneous analyses were produced, both by standards-based EDS on an SEM and WDS on an electron microprobe.

Interest in Fe L lines is nothing new in EPMA. Early interest focused upon changes in peak shape and position between Fe metal and Fe oxides (Fischer, 1965). Anderson (1967) in a review of soft X-ray EPMA, included a study of the use of three Fe L lines: Fe-L α , Fe-L β , and Fe-LI. He used pure Fe and Fe₃O₄ standards to quantify the Fe in two Fe oxides, FeS₂ and Fe₃C, and noted major problems. O'Nions and Smith (1971) evaluated Fe L α - L β spectra of a variety of minerals with different oxidation states in the hope of using EPMA to easily determine Fe³⁺/Fe²⁺ ratios. The results were not encouraging. All of these studies refer to the issue of carbon contamination and of surface artifacts having a deleterious role. They have ranged from describing the detailed electron structure of iron compounds, to being able to determine the ferrous to ferric iron ratio in minerals of interest to geologists.

Methods

Analyses were first conducted at the Eugene Cameron Electron Microprobe Laboratory (UW Madison) using a CAMECA SX-51 electron microprobe (W filament source, operated at 5 keV) and Probe for EPMA software (Donovan et al., 2012). Initial data obtained on the Fe-Si reference materials (mounted in epoxy and coated with an ~ 200 Å carbon coating) using the Fe L α and Si K α lines returned ~ 120 wt.% totals. In each case the Fe wt.% was anomalously ~ 20 wt.% high). In all cases we used the same high purity metals as standards (99.99 % Fe, and 99.9 % Si). The metal standards were mounted in each Fe-Si block. To validate the high wt.% totals, a sample mount with the Fe-Si reference materials was sent to the University of Barcelona to be analyzed there on a CAMECA SX-50. Also, the reference materials, as well as the lunar grain, were analyzed on the prototype CAMECA SX-5 FE, located in Fitchburg, Wisconsin, at the time. Similar erroneous results were obtained on all machines.

Our approach was to obtain several synthetic Fe-silicides with well determined compositions, then study the possible factors involved in the inaccurate Fe compositional determinations, initially focusing on (1) chemical peak shifts, (2) comparing usage of the 3 possible crystal diffractors: TAP, PC0, PC1 (count rates versus spectral resolution), and (3) MACs.

The Fe-Si samples had to be large enough to be analyzed with a tungsten source. Some were supplied by a colleague (Heikinheimo, E., Aalto University, Espoo, Finland). Others were synthesized in the UW-Madison Departments of Material Science and Chemistry. Fe:Si ratios in the synthetic samples were chosen to ensure that the full range of compositions in the Fe-Si

system were covered. Samples were first weighed as a powder, using reagent grade material, then pressed into pellets. The pellets were then transferred to an arc-melter, where the samples were arc-melted three times. The entire procedure (weighing, pressing, and arc melting) was carried out in an argon-filled glove-box to minimize oxidation.

Multiple samples of each phase were synthesized. The samples were annealed at either 900°C or 1125°C for a month at a time until each sample was deemed fully homogenous (figure 5). After each month of annealing one of the samples from each phase was quenched, cut in half, and checked with high contrast backscattered electron imaging (on a Hitachi S3400-N scanning electron microscope) to verify phase homogeneity. The reference materials were then analyzed with the UW Madison CAMECA SX-51 at 15 keV to determine the composition of the reference materials, as there is some solid solution in some of the phase fields.

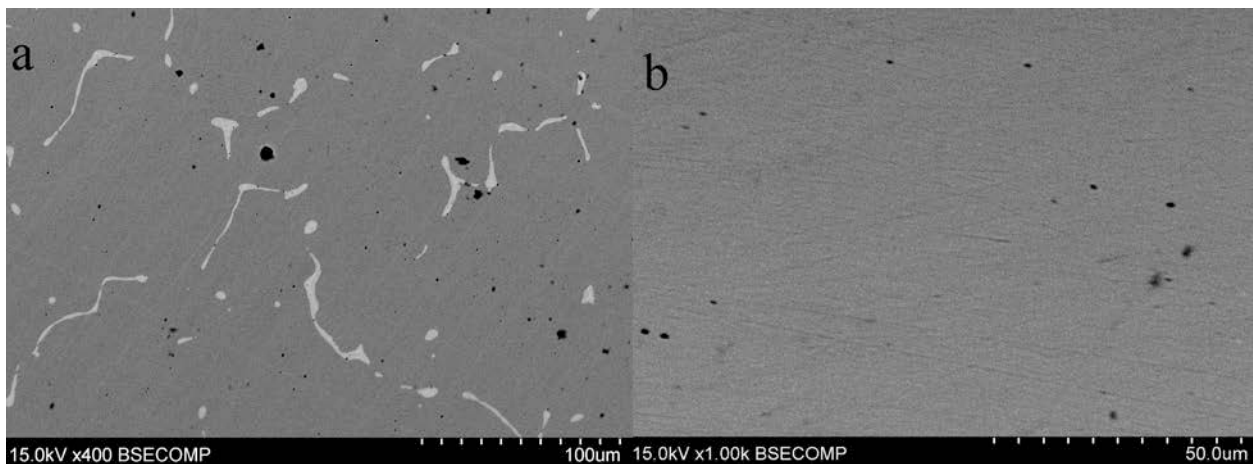


Figure 5: BSE images of FeSi after 1 week (a) and 4 weeks (b) annealing at 1100°C.

The Fe-Si reference materials mounted in electrically conductive indium (so as the samples could remain uncoated) were then quantitatively analyzed using 5 keV/100 nA using both the Fe $L\alpha$ and $L\beta$ lines. By analyzing an uncoated sample at 100 nA with short count times (20 seconds on peak/ 10 seconds on the background) we avoided most of the time dependent effects of the carbon buildup. Alternatively a time dependent intensity (TDI) correction, such as that used in the Probe for EPMA software (Donovan et al., 2012) could be used; however it was not needed in the case of our analyses because of the care taken to avoid carbon coated samples. The iron wt.% was closer to the nominal composition, but still high (Table 1).

Fialin et al. (1998) suggested the use of $L\eta$ and $L\theta$ lines, as alternatives to the normally used $L\alpha$ and $L\beta$ lines. As none of the commercially available electron probe software allows for the use of $L\eta$ lines for quantitative analysis, an alternative method was used to test the feasibility of the Fe $L\eta$ line for quantitative EPMA. The raw counts were obtained on the UW Madison CAMECA-SX 51, using the Probe for EPMA software, and “mispeaking” the Fe $L\alpha$ line on the $L\eta$ line. The K-ratios obtained were then run through the Pouchou and Pichoir (PAP) model (Pouchou and Pichoir, 1984) matrix corrections in "Son of Desktop Spectrum Analyzer" (DTSA II) (Ritchie, 2009). The quantification tool in DTSA II does not allow for use of $L\eta$ lines; however, in the newest version of the software (Gemini), a command window is available for implementing a desired code. Phillippe Pinard at RTWH Aachen (Germany), wrote a script for

DTSA II that allowed the quantification of L1 lines. This code was then used to determine the compositions of our Fe-Si compounds, with the K-ratios determined in Probe for EPMA.

After the groundwork to develop the technique to analyze sub-micron phases, we were able to analyze lunar Fe-Si using a JEOL 8530 FE at the RWTH University Aachen and another JEOL 8530 FE at ExxonMobil Research and Engineering Corporation. Care was taken to reduce the carbon contamination on the sample prior to analysis, because we were interested in the carbon concentration in the Fe-Si blebs.

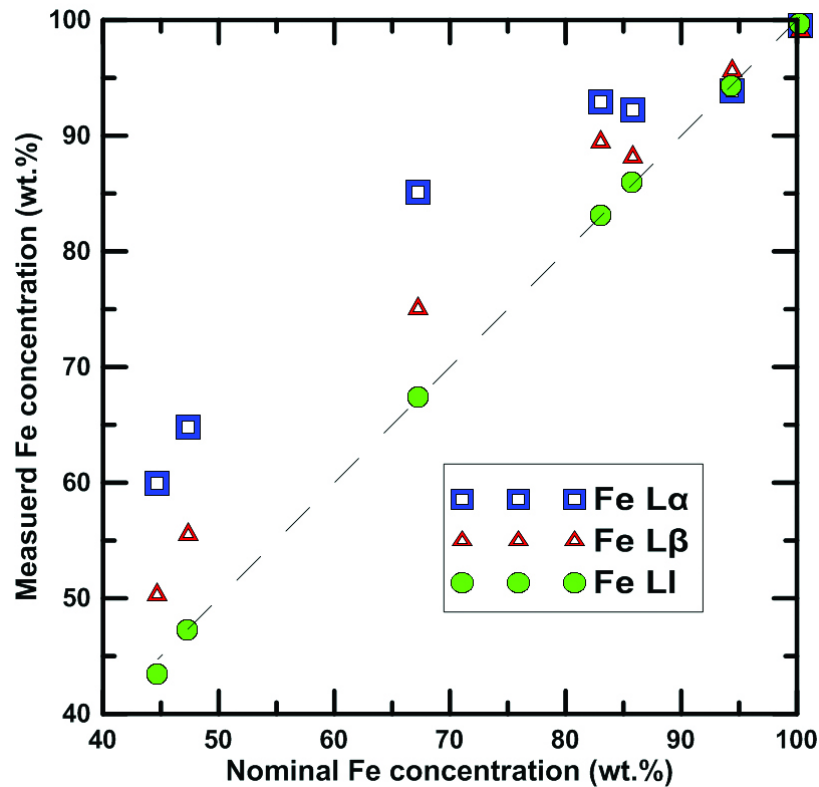


Figure 6: Measured at low voltage versus nominal (as measured at 15 keV with Fe K α ; dashed line) Fe concentrations obtained on the various Fe-Si reference materials, in the epoxy mount coated with platinum. Fe L α and L β were acquired and quantified in Probe for EPMA, using the full PAP matrix correction. Fe L1 was acquired in Probe for EPMA, but quantified in DTSA II using the PAP model.

Results

Table 1 shows the results of using the Fe L α , L β , and L1 lines, as well as different MACs, for the analysis of Fe-Si compounds, at 5 keV. The data with the greatest deviation from the nominal composition is that acquired with the Fe L α line. The Fe L β line gives Fe wt.% closer to nominal, but still off by over 10 wt.% for Fe₃₀Si₇₀. The Si wt.% obtained at 5 keV are systematically higher than those obtained at 15 keV by a factor ranging from 1.03-1.05, except for the Fe₉₀Si₁₀ alloy. This discrepancy is probably due to measurement difficulty combined with a change in the matrix correction with the incorrect Fe concentration. The effect of using different MACs is noticeable (~ 2 wt% difference in Fe counts), but is not enough to correct for the large errors in Fe numbers using the Fe L α and L β lines. Using the Fe L1 line (L₃-M₁ transition), in conjunction with the DTSA II, for quantitative analysis gives compositions closer to the nominal values, even whilst using pure metals as standards.

| | At % | | MAC | La | | | Lβ | | | Ll | | |
|------------------|---------|-----------|--------|--------|--------|-----------|--------|--------|-----------|--------|--------|-----------|
| | Wt % | Wt% 15keV | | Fe wt% | Si wt% | Total wt% | Fe wt% | Si wt% | Total wt% | Fe wt% | Si wt% | Total wt% |
| Fe90 Si10 | Fe94.71 | Si5.20 | Henke | 94.22 | 4.95 | 99.17 | X | X | X | X | X | X |
| | | | Heinr. | 94.21 | 4.95 | 99.16 | 95.50 | 5.04 | 100.53 | 94.37 | 4.99 | 99.36 |
| | | | Chant. | 94.26 | 4.95 | 99.21 | 95.89 | 5.04 | 100.92 | 94.33 | 4.95 | 99.28 |
| | | | Sokar. | 93.87 | 4.95 | 98.82 | 95.64 | 5.04 | 100.68 | X | X | X |
| | | | Gopon | 93.86 | 4.95 | 98.81 | 94.80 | 5.04 | 99.84 | X | X | X |
| Fe75 Si25 | Fe85.64 | Si14.36 | Henke | 93.16 | 13.85 | 107.02 | X | X | X | X | X | X |
| | | | Heinr. | 93.16 | 13.85 | 107.01 | 87.76 | 14.26 | 102.02 | 86.14 | 13.99 | 100.13 |
| | | | Chant. | 93.27 | 13.85 | 107.13 | 88.81 | 14.26 | 103.07 | 86.01 | 13.87 | 99.88 |
| | | | Sokar. | 92.28 | 13.85 | 106.13 | 88.15 | 14.26 | 102.42 | X | X | X |
| | | | Gopon | 92.27 | 13.85 | 106.12 | 85.84 | 14.26 | 100.11 | X | X | X |
| Fe70 Si30 | Fe82.27 | Si17.73 | Henke | 93.97 | 17.03 | 111.01 | X | X | X | X | X | X |
| | | | Heinr. | 93.97 | 17.03 | 111.00 | 88.94 | 18.22 | 107.16 | 83.25 | 17.21 | 100.46 |
| | | | Chant. | 94.11 | 17.03 | 111.14 | 90.26 | 18.22 | 108.48 | 83.11 | 17.07 | 100.18 |
| | | | Sokar. | 92.92 | 17.04 | 109.96 | 89.44 | 18.22 | 107.66 | X | X | X |
| | | | Gopon | 92.91 | 17.04 | 109.95 | 86.53 | 18.22 | 104.75 | X | X | X |
| Fe50 Si50 | Fe66.54 | Si33.46 | Henke | 86.80 | 32.99 | 119.79 | X | X | X | X | X | X |
| | | | Heinr. | 86.79 | 32.99 | 119.78 | 74.25 | 34.40 | 108.65 | 67.57 | 33.45 | 101.02 |
| | | | Chant. | 87.01 | 32.99 | 120.00 | 76.45 | 34.39 | 110.85 | 67.37 | 33.22 | 100.59 |
| | | | Sokar. | 85.11 | 33.01 | 118.12 | 75.08 | 34.40 | 109.48 | X | X | X |
| | | | Gopon | 85.09 | 33.01 | 118.10 | 70.09 | 34.42 | 104.51 | X | X | X |
| Fe33 Si67 | Fe49.82 | Si50.18 | Henke | 66.88 | 52.51 | 119.39 | X | X | X | X | X | X |
| | | | Heinr. | 66.86 | 52.51 | 119.38 | 54.47 | 53.93 | 108.41 | 47.41 | 53.31 | 100.72 |
| | | | Chant. | 67.13 | 52.51 | 119.64 | 57.23 | 53.90 | 111.13 | 47.23 | 53.06 | 100.29 |
| | | | Sokar. | 64.85 | 52.56 | 117.41 | 55.53 | 53.92 | 109.44 | X | X | X |
| | | | Gopon | 64.83 | 52.56 | 117.39 | 49.25 | 54.00 | 103.25 | X | X | X |
| Fe30 Si70 | Fe46.01 | Si53.99 | Henke | 61.96 | 55.96 | 117.92 | X | X | X | X | X | X |
| | | | Heinr. | 61.94 | 55.96 | 117.90 | 47.86 | 56.57 | 104.43 | 43.62 | 56.78 | 100.40 |
| | | | Chant. | 62.21 | 55.96 | 118.17 | 50.54 | 56.53 | 107.06 | 43.45 | 56.54 | 99.99 |
| | | | Sokar. | 59.94 | 56.02 | 115.96 | 50.36 | 57.25 | 107.60 | X | X | X |
| | | | Gopon | 59.53 | 56.02 | 115.55 | 42.79 | 56.65 | 99.44 | X | X | X |

Table 1: Comparison of Fe La, Lβ, and Ll and the effect of different MACs for quantitative EPMA at 5 keV. Fe La and Lβ were acquired and quantified in Probe for EPMA, using the full PAP matrix correction. Fe Ll was acquired in Probe for EPMA, but quantified in DTSA II using the full PAP matrix correction. The Ll data only shows results for Heinrich and Chantler because DTSA II only allows for use of those two MAC tables. At the top of each composition (black background) is both the nominal composition of the phase (left), and the composition as measured at 15 keV (right) using the Fe Kα line with the LIF crystal, the PAP matrix correction, and the Chantler MACs. All data was acquired on a platinum coated block of our Fe-Si standards, with the exception of the 15 keV data which was acquired in the same block when it had a carbon coating.

Figure 6 graphically shows the improvement in the measurements, using the various Fe L lines. One possible explanation for the better results obtained by using the Fe L η line is that this line is the furthest L line away from the L $_3$ absorption edge (figure 3), and unlike the L β line, it has a relatively low MAC, and should not be affected by near-edge absorption effects. Moreover, the L $_3$ -M $_1$ transition involves electron orbitals other than the 3d which are not involved in chemical bonding (figure 2), thus keeping an “atomic-like” character.

The Fe L η X-ray lines do not yield high count rates (relative to those of Fe L α /L β). Low count rates mean that either more current or longer counting times (or both) must be used to get statistically significant data. Longer counting times and higher currents lead to larger surface effects being produced over the course of the analysis. This may lead to changing counts on the various samples. Given that the Fe L η (L $_2$ -M $_1$ transition) has virtually the same character as that of the L η line, their combination should not be critical. Even though the Fe L η line has the lowest count rates out of the three possibilities being investigated (L α , L β , and L η lines), it appears to be the best X-ray line for quantitative EPMA at low voltage. Fialin et al (1998) however, already made the prescient suggestion related to the transition metals, that “Despite their low intensities, the ‘atomic’ L η peaks (3s-2p transition) are more convenient [than L α - β] for those applications to [EPMA] practice.”

Figure 7 shows the results of our EPMA data acquired on the JEOL 8350 FE. We found appreciable carbon concentrated in the Fe-Si blebs. Due to concern over contamination we do not know exactly how much carbon is present in the Fe-Si, but the X-ray maps of carbon clearly show that the carbon is concentrated in the Fe-Si. While iron metal is common on the moon as a product of micro-meteorite impacts, the conditions for silicon metals and iron-silicides to occur are an order of magnitude more reducing. The presence of carbon would explain how such a highly reduced phase could have formed on the moon. A carbonaceous impactor is a likely scenario as to how the carbon ended up in the Fe-Si blebs. The meteorite would have impacted the lunar surface and locally vaporized the lunar surface. The vacuum of the lunar environment would have reduced the vapor cloud to a large degree, but the presence of carbon in the vapor would have scavenged the remaining oxygen and allowed for the extreme reducing conditions required to form the iron-silicides.

Conclusions

Currently one of the factors holding back full application of the low voltage, high spatial resolution EPMA (e.g. field emission EPMA) is the “energy barrier” raised by usage of the traditional X-ray analytical lines, e.g. Fe K α . We have demonstrate that non-traditional lines such as Fe L η can provide significant improvements in EPMA of iron silicides at low voltages. Additionally, fully quantitative EPMA using standards with un-normalized totals must be utilized as the analytical total is a critical tool for quality control of micro-analytical results. Using this new technique for analysis of sub-micron phases we were able to quantitatively measure the Fe-Si blebs and determine that they contained an appreciable amount of carbon. This finding provides new interesting insight into lunar geology.

Table 2: Results of quantitative analysis on Fe-Si blebs in lunar grain A6-8. Note the carbon measurements in blebs 1-5 are compromised because of contamination.

| Bleb # | Fe | Si | Ni | Al | C | P | S | Total |
|--------|-------|--------|-------|------|-------|------|------|--------|
| 1 | 47.10 | 27.68 | 5.91 | 0.63 | 17.81 | 0.14 | | 99.26 |
| 2 | 30.28 | 40.44 | 3.77 | 1.63 | 23.37 | 0.11 | | 99.59 |
| 3 | 35.97 | 43.31 | 4.45 | 0.69 | 17.63 | 0.13 | | 102.18 |
| 4 | 41.44 | 48.98 | 2.80 | 0.61 | 4.70 | 0.20 | 0.05 | 98.78 |
| 5a | 26.77 | 50.30 | 6.83 | 1.02 | 9.53 | 2.22 | 0.13 | 96.81 |
| 5b | 0.00 | 91.19 | 0.03 | 0.88 | 15.08 | 0.74 | 0.04 | 107.96 |
| 6 | 0.00 | 97.48 | 0.00 | 0.16 | 2.90 | 0.88 | 0.00 | 101.41 |
| 7 | 0.00 | 97.25 | 0.09 | 0.16 | 4.30 | 1.20 | 0.04 | 103.03 |
| 8 | 37.04 | 50.87 | 3.58 | 2.39 | 4.47 | 1.27 | 0.06 | 99.68 |
| 9 | 32.57 | 49.24 | 12.50 | 1.14 | 3.17 | 0.48 | 0.02 | 99.12 |
| 10 | 34.10 | 51.89 | 8.38 | 0.83 | 2.87 | 0.70 | 0.07 | 98.85 |
| 11 | 0.00 | 94.33 | 0.18 | 0.29 | 19.42 | 1.22 | 0.03 | 115.46 |
| 12a | 0.00 | 101.38 | 0.10 | 0.29 | 4.21 | 0.97 | 0.04 | 106.99 |
| 12b | 35.68 | 53.09 | 4.43 | 0.32 | 7.50 | 3.55 | 0.02 | 104.59 |
| 13a | 39.79 | 55.38 | 4.53 | 0.73 | 4.64 | 0.83 | 0.01 | 105.91 |
| 13b | 0.00 | 95.75 | 0.11 | 0.86 | 15.19 | 0.69 | 0.04 | 112.64 |
| 14a | 39.89 | 54.09 | 3.93 | 0.92 | 5.83 | 0.41 | 0.03 | 105.10 |
| 14b | 37.65 | 54.06 | 3.60 | 0.80 | 7.30 | 0.12 | 0.03 | 103.55 |
| 15 | 25.52 | 50.23 | 27.76 | 1.18 | 5.84 | 1.38 | 0.09 | 111.99 |
| 16 | 14.86 | 50.61 | 23.98 | 1.55 | 4.19 | 0.69 | 1.93 | 97.81 |
| 17 | 25.22 | 50.95 | 9.97 | 2.57 | 4.75 | 1.60 | 0.11 | 95.17 |

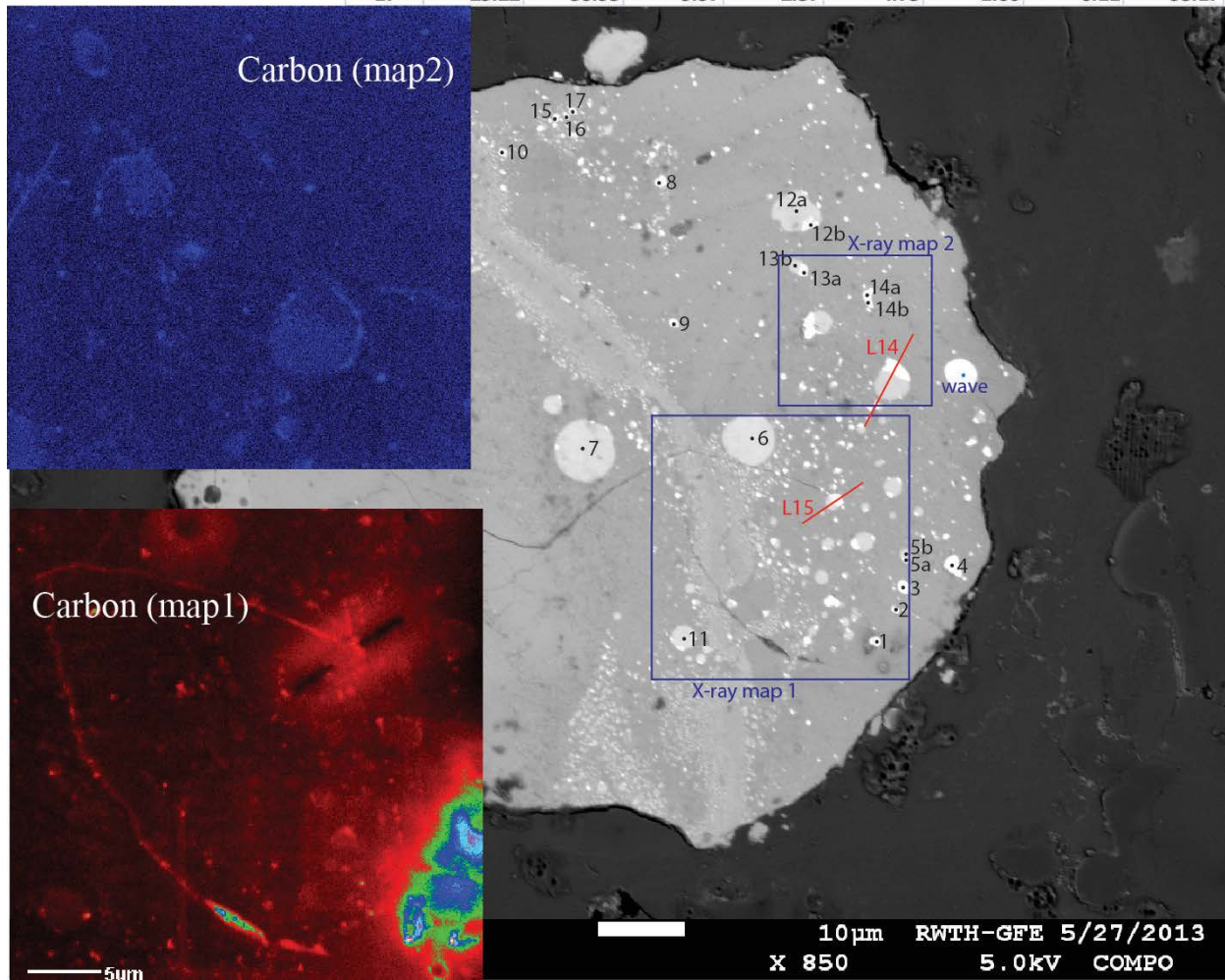


Figure 7: BSE image of lunar grain A6-8 showing location of quantitative analyses as well as locations of X-ray maps, with the carbon maps for each shown on the left.

References

- ANDERSON, C. A. (1967). The quality of x-ray microanalysis in the ultra-soft x-ray region. *Bri. J. Appl. Phys.* **18**, 1033–1043.
- ANAND, M., TAYLOR, L. A., NAZAROV, M. A., SHU, J., MAO, H.K., & HEMLEY, R. J. (2004). Space weathering on airless planetary bodies: clues from the lunar mineral hapkeite. *Proc. Natl. Acad. Sci. U. S. A.* **101**, 6847–51.
- ARMSTRONG, J. (2011). Low voltage and low overvoltage X-ray nanoanalysis with field emission electron microprobes and SEMs: Problems in quantitation for first-row transition elements. 2011 AGU Fall Meeting, San Francisco, CA.
- CASTAING, R. (1951). Application of electron probes to local chemical and crystallographic analysis. Thesis, University of Paris 1951 Publication *O.N.E.R.A No. 55* (1952).
- CHANTLER, C. T., OLSEN, K., DRAGOSET, R.A., CHANG, J., KISHORE, A.R., KOTOCHIGOVA, S.A., ZUCKER, D.S. (2005). X-ray form factor, attenuation, and scattering tables. Retrieved from www.nist.gov/pml/data/ffast/index.cfm.
- DONOVAN, J.J., KREMSE, D., FOURNELLE, J., & GOEMANN, K. (2012), *Probe for EPMA: Users Guide and Reference*. 438 pp. Available online as pdf at ProbeSoftware.com.
- DROUIN, D., COUTURE, A. R., JOLY, D., TASTET, X., AIMEZ, V. & GAUVIN, R. (2007). CASINO V2.42: a fast and easy-to-use modeling tool for scanning electron microscopy and microanalysis users. *Scanning* **29**, 92–101.
- ESSENE, E. J. & FISHER, D. C. (1986). Lightning strike fusion: extreme reduction and metal-silicate liquid immiscibility. *Science (New York, N.Y.)* **234**, 189–93.
- FIALIN, M., WAGNER, C., REMOND, G. (1998). X-ray emission valence band spectrometry: application to cu and fe L-series. In *EMAS* **98**, 129–140.
- FISCHER, D. W. & BAUN, W. L. (1967). Self-absorption effects in the soft X-Ray $M\alpha$ and $M\beta$ emission spectra of the rare earth elements. *J. Appl. Phys.* **38**, 4830–4836.
- GOPON, P., FOURNELLE, J., LLOVET, X. (2012). Soft X-ray EPMA of submicron phase lunar Fe-Si compounds: *Microsc. Microanal.* **18** (Suppl 2) 1728-1729.
- GOPON, P., SOBOL, P.E. (2012). Non-sequential spectral acquisitions to remove time or dose dependent effects. *Unpublished report*.
- HEINRICH, K.F.J., (1987). Mass attenuation coefficients for electron microprobe microanalysis. in *Proc. 11th ICXOM*, 67-119.
- HEINRICH, K. F. J. (1964). X-ray absorption uncertainty. In McKinley T.D., ed., *The electron microprobe*, 296–377. New York: John Wiley & Sons.
- HENKE, B.L., LEE, P., TANAKA, T.J., SHIMABUKRO, R.L., FIJIKAWA, B.K. (1982) *Atomic Data Nucl. Data Tables* **27**, 1.
- HENKE, B. L., WHITE, R. & LUNDBERG, B. (1957). Semi-empirical determination of mass absorption coefficients for the 5 to 50 angstrom X-Ray region. *J. Appl. Phys.* **28**, 98.
- LLOVET, X., HEIKINHEIMO, E., NÚÑEZ, A., MERLET, C., ALMAGRO, J., RICHTER, S., FOURNELLE, J. & VAN HOEK, C. (2012). An inter-laboratory comparison of EPMA analysis of alloy steel at low voltage. In *IOP Conf. Ser.: Mater. Sci. Eng.* **32**. 1-14.
- MACKENZIE, A.P. (1993). Recent progress in electron-probe microanalysis. *Rep. Prog. Phys.* **56**, 557–604.
- O'NIONS, R.K., SMITH, D.G.W. (1971) Investigation the $L_{II, III}$ emission spectra of Fe by electron microprobe: Part 2. The Fe $L_{II, III}$ spectra of Fe and Fe-Ti oxides, *Am. Mineral.*, **56**, 1452-1455.
- POUCHOU, J. L. (1996). Use of soft X-rays in microanalysis. *Mikrochim. Acta (Suppl.)* **12**, 39–60.
- POUCHOU, J. L., PICOIR, F., & BOIVIN, D. (1990). XPP procedure applied to quantitative EDS x-ray analysis in the SEM,” in *Microbeam Analysis* (San Francisco, San Francisco), pp. 120–126.
- POUCHOU, J. L., PICOIR, F., (1984). A New Model for Quantitative X-Ray Microanalysis. I.--Application to the Analysis of Homogeneous Samples. *Rech. Aerosp.*, (3), 167-192.
- RIETMEIJER, F., NAKAMURA, T., TSUCHIYAMA, A., UESUGI, K., NAKANO, T. & LEROUX, H. (2008). Origin and formation of iron silicide phases in the aerogel of the Stardust mission. *Meteoritics and Planet. Sci.* **1/2**, 121–134.
- RITCHIE, N.W.M. (2009). Spectrum simulation in DTSA-II. *Microsc. Microanal.* **15**, 454-468.
- SOKARAS, D., KOCHUR, A., MÜLLER, M., KOLBE, M., BECKHOFF, B., MANTLER, M., ZARKADAS, C., ANDRIANIS, M., LAGOYANNIS, A. & KARYDAS, A. (2011). Cascade L-shell soft-x-ray emission as incident x-ray photons are tuned across the 1s ionization threshold. *Phys. Rev. A* **83**, 1–12.
- SPICUZZA, M. J., VALLEY, J. V., FOURNELLE, J., HUBERTY, J. M. & TREIMAN, A. (2011). Native silicon and Fe-silicides from the Apollo 16 lunar regolith: Extreme reduction, metal-silicate immiscibility, and shock melting. In *42nd Lunar and Planet. Sci. Conf. (2011)* **97**, 16–17.